



This is a repository copy of *Investigation of ferrofluid cooling for high power density permanent magnet machines*.

White Rose Research Online URL for this paper:

<https://eprints.whiterose.ac.uk/193666/>

Version: Accepted Version

---

**Article:**

Zhang, W., Li, G.-J. [orcid.org/0000-0002-5956-4033](https://orcid.org/0000-0002-5956-4033), Ren, B. et al. (2 more authors) (2023) Investigation of ferrofluid cooling for high power density permanent magnet machines. IEEE Transactions on Magnetics, 59 (1). 4600211. ISSN 0018-9464

<https://doi.org/10.1109/TMAG.2022.3224787>

---

© 2022 IEEE. Personal use of this material is permitted. Permission from IEEE must be obtained for all other users, including reprinting/ republishing this material for advertising or promotional purposes, creating new collective works for resale or redistribution to servers or lists, or reuse of any copyrighted components of this work in other works. Reproduced in accordance with the publisher's self-archiving policy.

**Reuse**

Items deposited in White Rose Research Online are protected by copyright, with all rights reserved unless indicated otherwise. They may be downloaded and/or printed for private study, or other acts as permitted by national copyright laws. The publisher or other rights holders may allow further reproduction and re-use of the full text version. This is indicated by the licence information on the White Rose Research Online record for the item.

**Takedown**

If you consider content in White Rose Research Online to be in breach of UK law, please notify us by emailing [eprints@whiterose.ac.uk](mailto:eprints@whiterose.ac.uk) including the URL of the record and the reason for the withdrawal request.



[eprints@whiterose.ac.uk](mailto:eprints@whiterose.ac.uk)  
<https://eprints.whiterose.ac.uk/>

# Investigation of Ferrofluid Cooling for High Power Density Permanent Magnet Machines

W. Zhang, G. J. Li, *Senior Member, IEEE*, B. Ren, Y. C. Chong, and M. Michon

**Abstract**— This paper investigates an advanced thermal management method adopting ferrofluid for improving the end-winding cooling of permanent magnet (PM) machines. An oil-based liquid with nano-sized ferromagnetic particles (which is known as ferrofluid) is used to fill in the cavity around the end-windings. This is to establish an effective heat flux path between the end-winding that is often regarded as hot spot in electrical machines and the external cooling system, i.e., water jacket, to improve the cooling performance of the PM machines. This improvement does not only result from the higher thermal conductivity and thermal expansion of the nanofluid with metal particles, but also from strong thermomagnetic convection generated by the magnetic body force of the ferromagnetic particles within the ferrofluid. Multiphysics models considering the interaction between the electromagnetic field, the heat transfer and the fluid dynamics have been built to study the thermal performances a PM machine under different load conditions. Several factors affecting the thermomagnetic convection such as the temperature dependent magnetization curve of the ferrofluid, the concentration and different ferromagnetic materials as well as different current densities have been investigated to analyze their influences on cooling performance. One major finding is that, compared with other coolant without magnetic body force, the ferrofluid can significantly reduce machine peak temperature, e.g., by around 36.4 °C when the current density is 22.1 A/mm<sup>2</sup>.

**Index Terms**— Ferrofluid cooling, magnetic body force, nanofluid, PM machines, thermomagnetic convection.

## I. INTRODUCTION

Permanent magnet (PM) machines are widely used in various applications, e.g., electrical and hybrid electrical vehicles, aerospace and wind power, etc. This is because of their high torque/power density, high efficiency and good fault tolerant capability. However, although the rare-earth magnets such as NdFeB generally have high energy density, which is essential for high power density PM machines, they are often sensitive to temperature rise. If left unattended, the overheating of PMs will lead to their irreversible demagnetization, meaning a permanent reduction of their magnetization. In addition, temperature rise within electrical machines also have significant impact on the properties of coil insulations. As a rule of thumb, a 10°C temperature rise over the rated value would halve the insulation life [1]. In order to improve machine's power density but at the same time protect the vulnerable components such as windings, PMs and bearings from overheating so that they can operate during their designed life spans, thermal managements based on natural air and liquid cooling, forced air and liquid cooling, or radiation cooling are becoming more and more important [2-5].

Amongst all the cooling technologies, the forced cooling, particularly the forced liquid cooling is the most effective in reducing machine's temperature. As a result, they have

attracted significant attention from both academia and industry. Examples such as water jacket [6] and hollow-shaft rotary system [7] have been widely adopted in industry. They can effectively cool the active parts of the machine such as active windings and rotor magnets. However, they are much less effective in cooling the end-windings, which are often regarded as hot spot within the electrical machines. This is mainly due to the high thermal resistance between the end-windings and the housing or shaft where the cooling system is located. To address these shortcomings, direct forced air/liquid cooling with inlets and outlets on the endcaps or housing for rotor-mounted PM machines or axial-flux PM machines have been investigated and the results showed that they can dramatically reduce the end-winding peak temperature [8-11]. Oil spray or jet impingement cooling is another forced cooling technology that is efficient in extracting heat from the end-windings. The machine structure of oil spray or jet impingement cooling is simple because it does not require a separator sleeve in the airgap as the semi-flooded cooling, i.e. forced oil cooling [12]. Its simplicity and efficacy are highlighted in [13-16]. However, for the above active cooling technologies, machine components such as the end-windings are directly exposed to the high speed and pressure coolant. This can lead to accelerated insulation degradation and reduced reliability, and hence requires more frequent maintenance.

To avoid the direct contact between the high speed and pressure coolant and the end-windings, a liquid-carrying pipe (liquid driven by external pump), is directly placed onto the end-windings. This additional cooling channel with water jacket embedded in the housing can achieve a 25% end-winding temperature reduction [17]. Moreover, a rotor self-ventilated cooling with wafters and flow deflectors being mounted on the rotor has also been proposed in [18, 19] to reduce the end-winding temperatures. When the rotor rotates, a strong recirculating toroidal vortex air flow is generated in end-winding regions. This helps extract heat from the end-windings to the housing water jacket. Apart from the above active cooling technologies, other more "passive" cooling technologies such as potting materials with high thermal conductivity can also be used to replace the air in the end-winding regions to establish an effective heat removal path between the end-windings and the housing water jacket [20]. In recent years, another passive cooling technology based on ferrofluid (FF) has been proposed. Ferrofluid can be driven by external magnetic field, leading to the self-circulation of the coolant and a phenomenon called thermomagnetic convection. This means that the closed-circuit liquid supply equipped with mechanical pumps, filters, etc. used in the active cooling systems will not be needed, leading to reduced capital and

operating costs. Because of the above advantages, ferrofluid has initially been used for power electronics device cooling [21, 22] and transformer cooling [23-26]. Then, some prior works have been carried out to investigate the feasibility of adopting ferrofluid for cooling the end-windings of electrical machines [27]. It is worth noting that, the model in [27] did not account for the gravitational effect and temperature dependent properties of the ferrofluid, and hence has limited model accuracy. More accurate multiphysics models of PM machines with ferrofluid cooling will be developed in this paper, which consider the strong coupling between the electromagnetic field, the fluid dynamics and the heat transfer. Using these multiphysics models, the influence of ferrofluid properties such as concentration, magnetization and Curie temperature as well as electrical loading on machine cooling performances will be studied.

It is worth noting that, same as other passive cooling technologies such as the end-winding potting, the ferrofluid cooling can only improve the heat transfer inside the machine, particularly the end-winding region. Therefore, its efficiency will ultimately be limited by the cooling efficiency of the external cooling system, i.e., the heat transfer on the housing surface or inside the housing with water jacket, for example. To maximize the cooling efficiency of the ferrofluid cooling, this paper proposes a hybrid cooling system, which includes a passive ferrofluid cooling system in the end-winding region and a housing water jacket, as shown in Fig. 1. Here, a sleeve is used to separate the stator and rotor parts and it is located in the end-winding region. This helps prevent fluid leakage to the rotating rotor region.

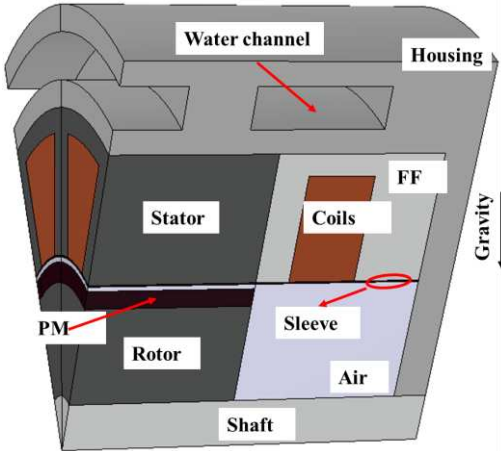


Fig. 1. PM machine with ferrofluid around end-windings and water jacket embedded in the housing. FF stands for ferrofluid.

## II. THEORETICAL BACKGROUND

Ferrofluid has seen a rapid development since it was first synthesized by Solomon Stephen Papell in 1963. It is often composed of nano-sized ferro- or ferrimagnetic particles and suspended in a liquid base. Typically, the diameter of nano-sized ferromagnetic particles is around 3~15 nm. This is because larger size of nanoparticles can reduce the suspension stability whilst smaller size (1~2 nm) can suppress their magnetic properties [28-30]. The properties of ferrofluid vary with the size of the nanoparticles, the concentration, the temperature and the applied external magnetic field. This will be detailed in the following sections.

### A. Properties of Ferrofluids

As mentioned above, the reason that ferrofluids can be used in machine cooling is that under an external magnetic field (often produced by the end-windings), the nanoparticles in the ferrofluid are subjected to a magnetic body force. This magnetic body force will drive the coolant, leading to thermomagnetic convection, which helps cool the end-windings. It is generally true that increasing this magnetic body force can enhance the cooling efficiency of the ferrofluid. The magnetic body force mainly depends on the applied external magnetic field and the magnetization of the ferrofluids.

To some extent, ferrofluids show superparamagnetic characteristics, one example of their magnetization curves is shown in Fig. 2. Its magnetization increases with increased external magnetic field strength, while the slope gradually reduces to near 0 when it reaches the saturation magnetization ( $M_0$ ) where all the dipoles in the ferrofluid are aligned with the external magnetic field. As the ferrofluid is often placed under relatively weak magnetic fields, the Langevin argument ( $\xi$ ) is much smaller than 1. According to Brillouin and Langevin law,  $\xi$  and the magnetization ( $M$ ) of a paramagnet can be described by [30, 31]

$$\xi = \frac{\mu_0 m H}{k_B T} \quad (1)$$

$$M = \chi H \quad (2)$$

where  $\chi$  is the magnetic susceptibility,  $\mu_0$  is the vacuum permeability,  $m$  is the magnetic moment of solute,  $H$  is the magnetic field strength,  $k_B = 1.38 \times 10^{-23}$  J/K is the Boltzmann constant, and  $T$  is the absolute temperature.

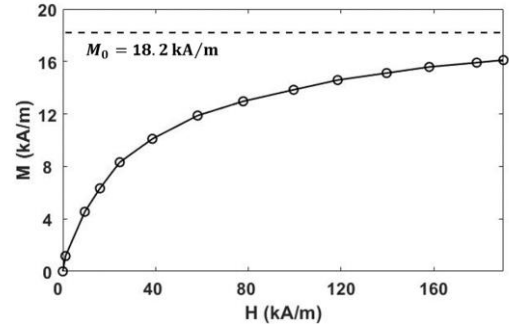


Fig. 2. Magnetization curve of ferrofluids used in [30].

By approximating the Langevin function,  $\chi$  of ferrofluid is given as [28]

$$\chi = \frac{\phi \mu_0 \pi d^3 M_{s,p}(T)^2}{18 k_B T} \quad (3)$$

where  $\phi$  and  $d$  are the volume fraction and average diameter of ferromagnetic particles, respectively.  $M_{s,p}(T)$  is the temperature dependent saturation magnetization, which can be derived by Bloch's law such as [24]

$$M_{s,p}(T) = \begin{cases} M_0 \left( 1 - \left( \frac{T}{T_c} \right)^{1.5} \right), & (\text{if } T \leq T_c) \\ 0, & (\text{if } T > T_c) \end{cases} \quad (4)$$

where  $M_0$  and  $T_c$  are the saturation magnetization at absolute zero kelvins and the Curie temperature of the ferromagnetic particles in the ferrofluid, respectively.

## B. Governing Equations

As mentioned before, the ferrofluid is often under weak magnetic field, where  $\xi \ll 1$  as derived in (1). As a result, the ferrofluid is considered as superparamagnetic fluid and its magnetic susceptibility can be derived by Langevin function. The behaviors of the ferrofluid in the investigated PM machines will be governed by the strong coupling between the magnetic field, the fluid dynamics and the heat transfer. And the governing equations will be explained in detail in the following sections.

### a. Fluid Dynamics

The behavior of flow is governed by Navier-Stokes equations and its time-varying model considering the body force is obtained by Bernoulli equation such as

$$\rho \frac{\partial \mathbf{u}}{\partial t} + \rho(\mathbf{u} \cdot \nabla)\mathbf{u} = \rho \mathbf{g} - \nabla p + \mathbf{F}_v + \mathbf{F}_m \quad (5)$$

where  $\mathbf{u}$  is the velocity vector,  $t$  is the time,  $\mathbf{g}$  is the acceleration of gravity vector and  $p$  is the pressure which is a function of temperature and density.

$\mathbf{F}_v$  in (5) is the viscosity force density vector dependent on the viscosity stress. For a compressible flow, the viscosity force density vector can be described by

$$\mathbf{F}_v = \eta \nabla^2 \mathbf{u} + (\lambda_\eta + \eta) \nabla(\nabla \cdot \mathbf{u}) \quad (6)$$

where  $\eta$  is the dynamic viscosity of the fluid and  $\lambda_\eta$  is the second coefficient of viscosity. In the classical theory, the second coefficient of viscosity is identified as  $-\frac{2}{3}\eta$  because the bulk viscosity coefficient should be 0.

$\mathbf{F}_m$  in (5) is the magnetic body force vector. It can be derived using different methods, including electrical current loop model, magnetic charge model and the Kelvin body force formula. They will be introduced in the following section.

### b. Electromagnetic Field

It is well established that the magnetic materials including ferromagnet, ferrimagnet and paramagnet will experience magnetic body force if they are put under an external magnetic field. Since the ferrofluid is regarded as a superparamagnetic solution and its susceptibility is independent of magnetic field intensity, the magnetic body force can be derived by the Kelvin body force formula such as [28]

$$\mathbf{F}_m = \mu_0 (\mathbf{M} \cdot \nabla) \mathbf{H} \quad (7)$$

### c. Heat Transfer

The heat transfer in solid and liquid can be described by

$$\nabla \cdot (\mathbf{q}) + Q = \rho C \frac{\partial T}{\partial t} \quad (8)$$

where  $\mathbf{q}$  and  $Q$  are the heat flux vector and volumetric heat generation. The heat flux vector for conduction ( $\mathbf{q}_s$ ) and convection ( $\mathbf{q}_f$ ) are described by [32]

$$\begin{cases} \mathbf{q}_s = \lambda \nabla T \\ \mathbf{q}_f = \rho C T \mathbf{u} \end{cases} \quad (9)$$

It is worth noting that, the heat flux vector for radiation has been neglected in this paper.

## III. MULTIPHYSICS MODELLING

The models of the ferrofluid for the end-windings cooling of the PM machines have been developed using COMSOL Multiphysics 5.6. However, as the water jacket does not have direct interaction with the ferrofluid cooling around the end-windings, in the thermal model, it has been replaced by a boundary condition using effective convection coefficient and effective coolant temperature on the housing surface, which have been calculated by ANSYS CFX 2020 R2. It is worth noting that, as the electrical time constant (a few ms) is much shorter than the hydrodynamics and thermal time constants, to ensure the model is solvable, the AC current in the models will be replaced by a DC current with the same RMS value. Similar approach has been adopted in [23, 24].

### A. Machine Topologies and Specifications

A conventional permanent magnet synchronous machine (PMSM) is used for the investigations in this paper. The topology is shown in Fig. 1. The specifications of this machine are listed in TABLE I. It is worth noting that, the gravity needs to be considered in the model and its direction is perpendicular to the rotor shaft as shown in Fig. 1. The ferrofluid will be filled in all the stator end-winding regions. To prevent the ferrofluid from leaking to the rotor end space, carbon sleeves are used to separate the stator and rotor end spaces.

TABLE I PARAMETERS OF THE PMSM MACHINE

Slot number	12	Stack length (mm)	50
Pole number	14	End-winding overhang (mm)	20
Stator outer radius (mm)	50	Housing radius (mm)	65
Stator yoke height (mm)	3.7	Housing length (mm)	120
Tooth width (mm)	7.1	Housing thickness (mm)	10
Airgap length (mm)	1	Number of coils per phase	132
Rotor outer radius (mm)	27.5	Wire diameter (mm)	1.32
Rotor yoke thickness (mm)	15.5	Current density (A/mm <sup>2</sup> )	18.4
Magnet thickness (mm)	3	Rated speed (rpm)	400
Magnet remanence (T)	1.2		

### B. Ferrofluid Properties

The ferrofluid used in the simulations in this paper is the same as that used by S. Nasser El Dine *et al* in [23]. The liquid base for the ferrofluid is vegetable oil. The parameters of the ferrofluid are listed in Table II.

TABLE II PARAMETERS OF THE FERROFLUID

Particle volume fraction (%)	5.4
Particle average diameter (nm)	16
Magnetization (A/m)	$3.87 \times 10^5$
Curie temperature (K)	793
Density (kg/m <sup>3</sup> )	1115
Thermal conductivity (W/m · K)	0.186
Dynamic viscosity (Pa · s)	0.0787
Specific heat capacity (J/kg/K)	$1.685 \times 10^3$

### C. Assumptions and Boundary Conditions

For the PMSM machine investigated in this paper, it is found that the magnetic field in the end space region generated by the rotor PMs is much smaller than that generated by the armature currents, as shown in Fig. 3. Therefore, it is safe to assume that the magnetic field generated by the PMs would have negligible impact on the cooling performance of the ferrofluid around the end-windings. In order to reduce the simulation time and make multiphysics model solvable, the rotation of the rotor will not be considered in the modelling.

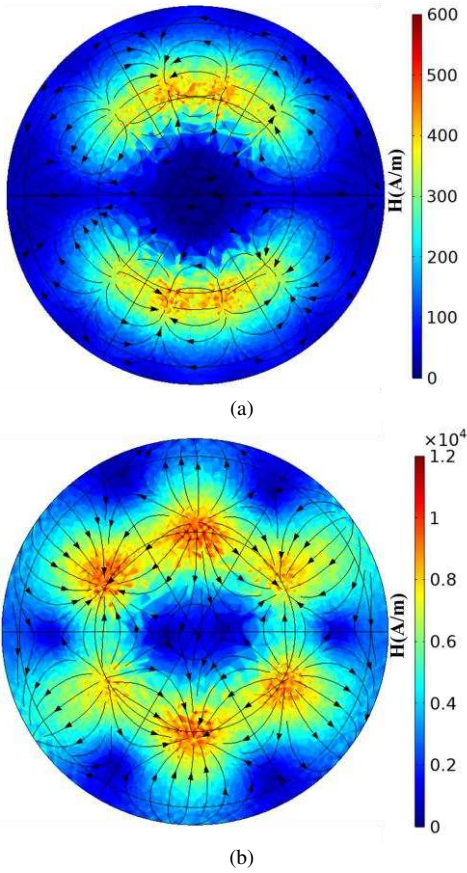


Fig. 3. Magnetic field strength distribution in the end space region. The plane chosen is the vertical plane [Plane 1 in Fig. 14 (a)], 5mm from the lateral surface of the end-winding. (a) Open circuit and (b) under rated current.

With different current densities, the magnetic field at end space has also been calculated as shown in Fig. 4. As one would expect, when current density increases, the magnetic field strength increases accordingly. This means that higher current will produce larger magnetic body force, and hence stronger magnetic cooling effect, as will be investigated in section IV.

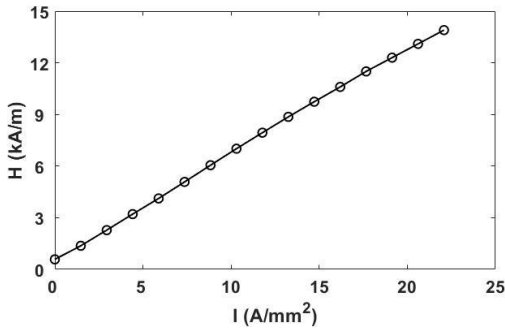


Fig. 4. Maximum magnetic field strength at the vertical plane [Plane 1 in Fig. 14 (a)], 5mm from the lateral surface of the end-winding.

For the computational fluid dynamics (CFD) modeling of the ferrofluid cooling, the boundaries of the fluid region are identified as no slip wall and the fluid velocity  $\mathbf{u}$  on the wall is 0 m/s. However, for the water jacket, its effective convection coefficient ( $h_e$ ) has been calculated by the CFD model using

$$h_e = \frac{Q}{T_{wall} - T_{ref}} \quad (10)$$

where  $Q$  is the average heat transfer rate per surface area from the machine inner regions to its housing.  $T_{wall}$  is the inner surface temperature of the housing and the reference temperature ( $T_{ref}$ ) is the average temperature of the coolant in the water jacket. Based on the CFD results, the boundary conditions applied to the multiphysics models developed in this paper are:

- On the housing active surface, the equivalent convection coefficient is 3718 W/m<sup>2</sup>/K and the reference temperature is 65°C.
- On the end-caps, the equivalent convection coefficient is 8 W/m<sup>2</sup>/K and the reference temperature is 20°C.

It is worth noting that the inlet flow rate for the water jacket is 1.37 L/min. This inlet flow rate has been chosen to achieve a reasonable total pressure loss (1200 Pa) and to ensure that the PM and coil temperatures at rated condition will not exceed their maximum allowable temperatures.

#### D. Mesh Sensitivity Tests

The number of mesh element for the model investigated in this paper is 341270. The time step is mutative, and the average value is around 1s to 2s. The model is solved for 8300 iterations (about 57 hours by 8 processors).

To investigate the influence of mesh size on the accuracy of the multiphysics model, different mesh sizes have been compared, as shown in Fig. 5. It is worth noting that as the ferrofluid region is the most important region for the multiphysics models, the analyses are focused on the mesh size in the ferrofluid region. The results show that reducing the average mesh size from 3.8mm<sup>3</sup> to 0.075mm<sup>3</sup> (the maximum mesh length reduces from 5mm to 1mm) will significantly increase the number of mesh elements by more than 8 times and the computation time by around 4.2 times. However, the temperature variation is only 0.3%. Therefore, the mesh size selected in this paper can be considered a reasonable compromise between the model accuracy and the computation time.

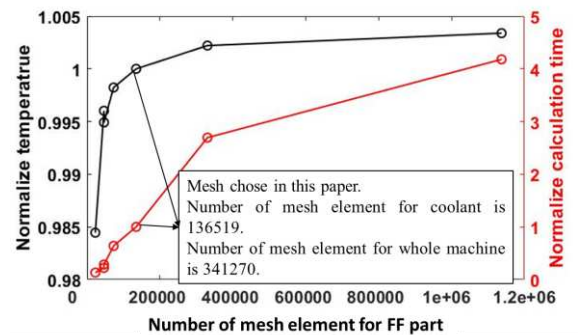


Fig. 5. Normalized maximum temperature and calculation time at different number of mesh elements (and different mesh sizes).

#### E. Model Validation

In order to validate the model accuracy, a multiphysics model of a transformer with ferrofluid cooling, exactly the same as that developed in [23], has been developed in this paper, as shown in Fig. 6. It is worth noting that, this model is a 2D axisymmetric model. In addition, the coil temperature variations against time (transient results) have also been compared, as shown in Fig. 7. A generally good agreement can be observed between the results obtained from the model

developed in [23] and the multiphysics model developed using COMSOL in this paper. It is worth mentioning that the model in [23] has already been validated by experiments. Therefore, a good agreement with the model in [23] can prove the accuracy of the model developed in this paper. Further model validation using experiments will be carried out in the section IV.

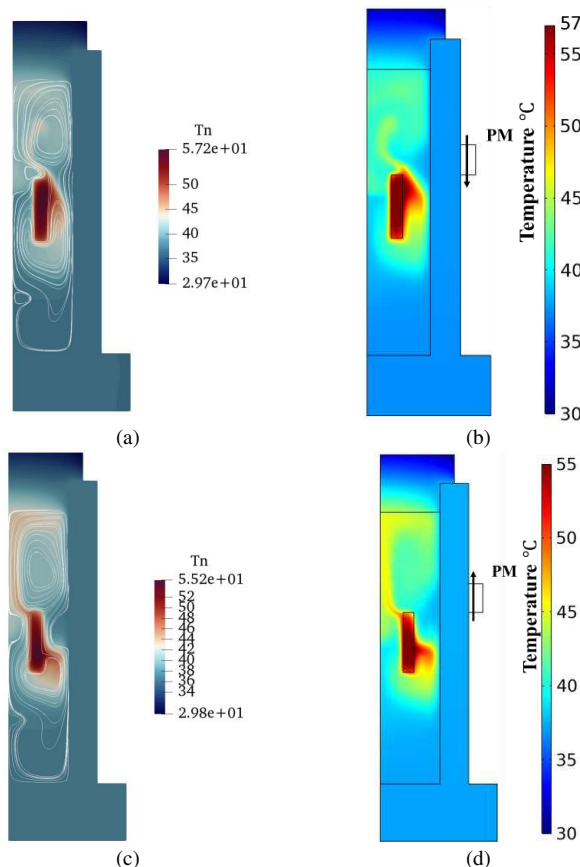


Fig. 6. Temperature distributions of transformers with annular magnet simulated (a) and (c) by the model developed in [23], and (b) and (d) by the model developed in this paper. The magnetization of the annular magnet is 0.3T in (a) and (b), and -0.3T in (c) and (d).

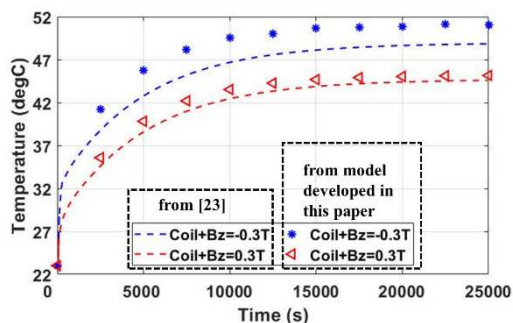


Fig. 7. Temperature variations against time of transformers with annular magnet obtained by model developed in [23] and model developed in this paper. The annular magnet has different magnetization directions, i.e.,  $B_z = 0.3T$  or  $-0.3T$ .

#### IV. EXPERIMENTAL VALIDATION

##### A. Motorette and Test Rig Setup

In order to further validate the multiphysics models, a motorette has been built, as shown in Fig. 8. The specifications of this motorette are listed in Table III. The geometries of stator lamination and housing are shown in Fig.

9 (a) and (b). An epoxy resin is used to fill the gaps between conductors, as well as the gap between the stator wall and the winding. This helps improve the equivalent thermal conductivity in the stator slots. A ferrofluid called AMG200-50 manufactured by Liquids Research Ltd has been used for the tests, and its properties are listed in Table IV. The water jacket [as shown in Fig. 9 (c)] is located at the back of the motorette. A commercial pump that can supply 1 L/min inlet flow rate to the water jacket is used for the tests.

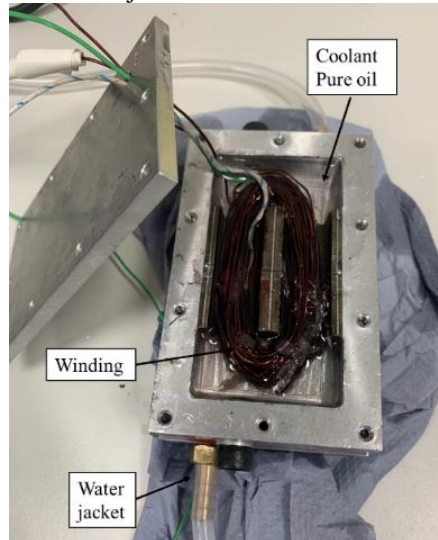


Fig. 8. Test motorette.

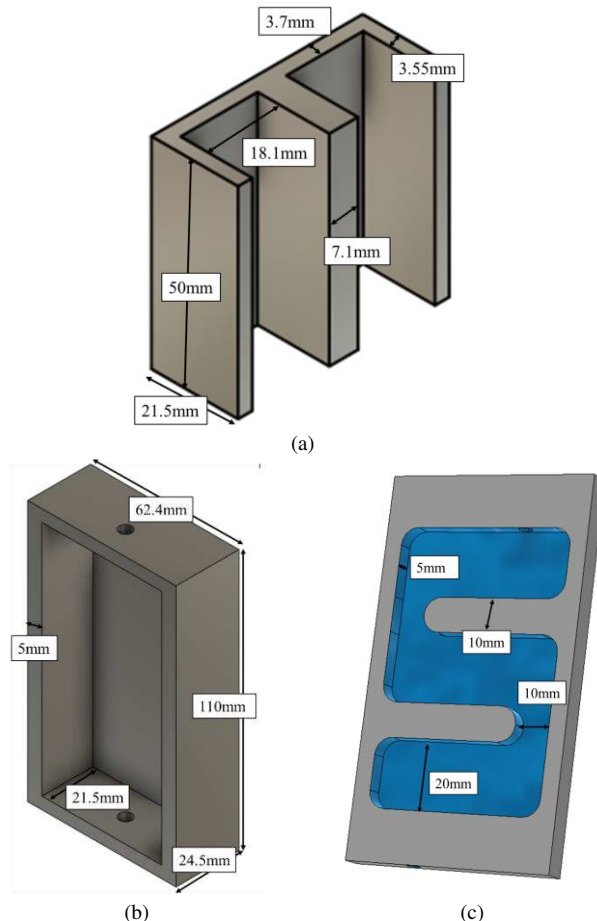


Fig. 9. (a) Stator lamination, (b) housing and (c) water jacket showing the details of the cooling channel.

TABLE III SPECIFICATION OF TESTED MOTORETTE

Stator width (mm)	50.4	Housing width (mm)	62.4
Stator height (mm)	50	Housing height (mm)	110
Stator depth (mm)	21.5	Housing depth (mm)	24.5
Slot depth (mm)	17.8	Housing thickness (mm)	5
Slot width (mm)	18.1	Number of turns	50

TABLE IV PARAMETERS OF THE FERROFLUID

Particle volume fraction (%)	$\approx 4$
Saturation Magnetization (A/m)	$1.54 \times 10^4$
Density at 25°C(kg/m <sup>3</sup> )	1100
Thermal conductivity (W/m · K)	0.15
Dynamic viscosity (Pa · s)	0.046
Initial permeability (at 30Oe)	1.68
Electrical resistivity (Ω/cm)	$> 10^9$
Heat capacity (J/kg/K)	1700

A test rig with the above motorette is built for the temperature measurements, as shown in Fig. 10. The end-winding temperature is measured using T-type thermocouples with an accuracy of  $\pm 0.5^\circ\text{C}$  and temperature results are recorded by Pico TC-08 thermocouple data logger.

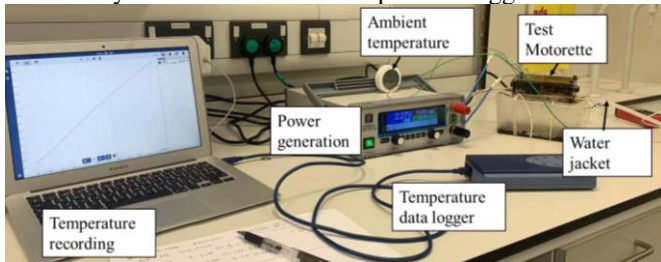


Fig. 10. Test rig.

## B. Temperature Measurements

Based on the motorette, a series of 3D multiphysics simulations have been carried out and will be compared against the measurements in this section. In the multiphysics models, the ambient temperature is set to be  $22^\circ\text{C}$  and the convection coefficient on the surfaces of the motorette is  $15\text{W/m}^2/\text{K}$ . The slot fill factor is 0.3, and the corresponding equivalent thermal conductivities of the winding are  $0.37\text{W/m/K}$  and  $120\text{W/m/K}$  in the directions that are perpendicular and parallel to the current, respectively.

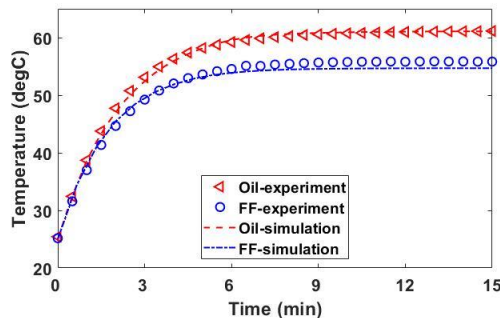


Fig. 11. Simulated and measured peak temperatures of the end-windings with oil and ferrofluid as coolant. The current injected into the coil is 10A.

A 10A dc current is injected into the coils of the motorette. It can generate 21.5W heat at room temperature ( $\approx 22^\circ\text{C}$ ). Under these conditions, the temperature of the end-windings has been simulated and measured for the motorette, as shown in Fig. 11. In order to verify the accuracy of the multiphysics simulations, both oil and ferrofluid have been used as coolant around the end-windings in the simulation and measurement. A very good agreement has been observed between the simulated and measured results, proving the accuracy of the

developed multiphysics model in this paper. In addition, as expected, a significant temperature reduction (by  $5.4^\circ\text{C}$ ) can be achieved when the ferrofluid is used to replace the oil as the coolant around the end-windings.

This significant temperature reduction is mainly due to the magnetic body force exerted on the nanoparticles in the ferrofluid, which significantly increases the coolant velocity. To show this phenomenon, two planes (Plane 1 and Plane 2) in the Multiphysics model have been chosen, as shown in Fig. 12. The velocity distributions for the motorette with oil and ferrofluid cooling are shown in Fig. 13. Due to magnetic body force (in ferrofluid), the coolant velocity is nearly twice as high as that without magnetic body force (in oil).

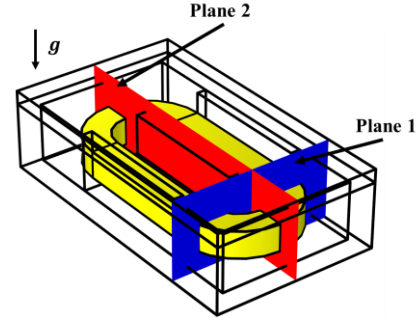


Fig. 12. Planes chosen to show the fluid dynamics results of the motorette.

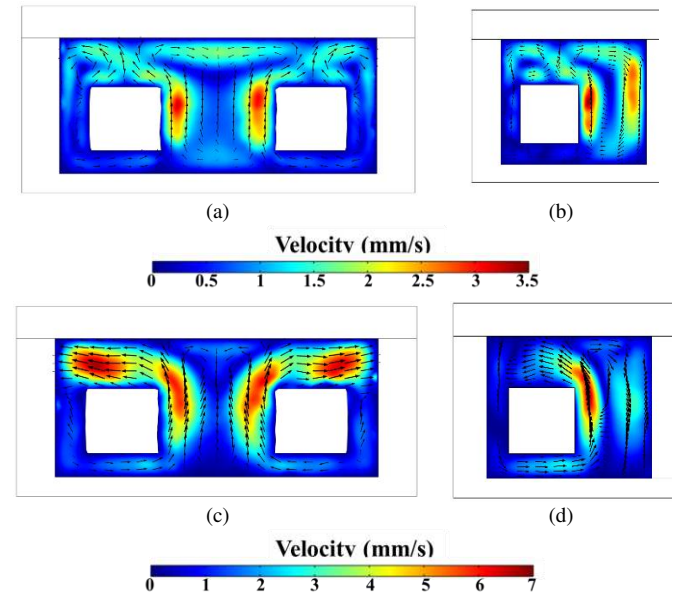


Fig. 13. Simulated results of coolant velocity on (a, c) plane 1 and (b, d) plane 2 for the motorette with (a, b) oil and (c, d) ferrofluid.

In addition, the steady-state peak temperature of the end-windings with ferrofluid as coolant has been measured and simulated for different currents. The measured and simulated results are listed in Table V. Again, regardless of the current levels, a good agreement can be observed between them.

TABLE V MEASURED AND SIMULATED TEMPERATURE OF THE MOTORETTE WITH FERROFLUID

Current (A)	Measured ( $^\circ\text{C}$ )	Simulation ( $^\circ\text{C}$ )	Difference (%)
5	32.0	33.1	3.4
6	35.7	36.5	2.2
7	40.0	40.3	0.75
8	44.1	44.4	0.68
9	48.8	49.2	0.81
10	55.8	54.6	2.1

## V. RESULTS AND DISCUSSIONS ABOUT THE PMSM

It is worth noting that, with proper adjustment, the previously validated Multiphysics models can be used to simulate the ferrofluid cooling in PMSM. This is mainly because the impact of rotor PMs of the PMSM can be negligible, as shown in Fig. 3. In addition, as the coils of the PMSM are single layer ones, the mutual inductive coupling between coils are also negligible. Therefore, the cooling effect of ferrofluid in the PMSM will be very much similar to the ones in the motorette.

In this section, two planes which are vertical (plane 1) and horizontal (plane 2) to the shaft are used to show the temperature distribution and fluid flow in the PMSM, as shown in Fig. 14 (a). Due to the gravitational effect, the temperature distribution and fluid flow are not circumferentially symmetrical, and they will be different around different end-windings. To clearly visualize this difference, in the post-process of the results, the end-winding region has been separated into 6 identical sections in axial direction and each span 60 degrees and has one coil in each section, as shown in Fig. 14 (b). The fluid dynamics and heat transfer results in each section will be investigated and compared in the following sections.

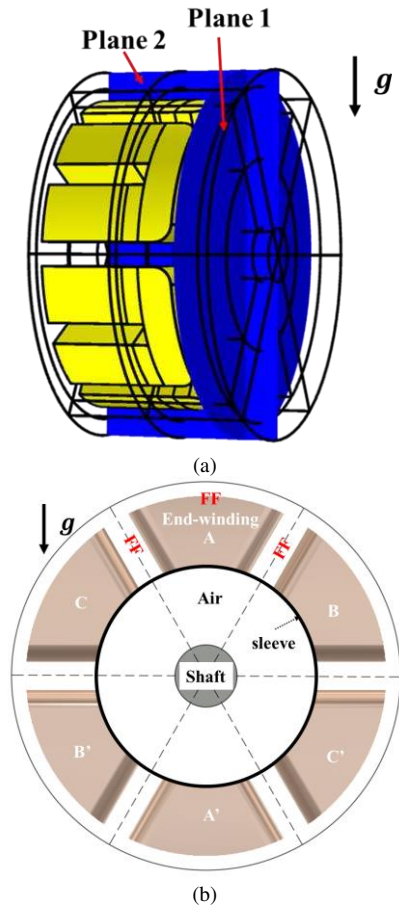


Fig. 14. (a) Planes chosen to show the temperature distribution and fluid flow and (b) six sections to analyze the fluid dynamics and heat transfer results.

### A. Different Coolants

The cooling performance of the ferrofluid has been compared against natural air and non-magnetic liquid such as nanofluid (liquid base + nanoparticles) and pure liquid base

without nanoparticles to show its capability in improving machine thermal performance. It is worth noting that, due to the insignificant gravitational effect, air is considered as incompressible fluid. In addition, the nanofluid has the same properties as the ferrofluid but does not have magnetic body force. This is to show the impact of the magnetic body force generated by the ferromagnetic particles in the ferrofluid. For different coolants, the peak coil temperatures versus time have been calculated using 3D COMSOL Multiphysics model, and the results are shown in Fig. 15. It is found that, when ferrofluid is introduced to replace air in the end-winding region, the peak coil temperature is reduced by 16.2°C. This temperature reduction is due to two factors, i.e., gravitational effect and magnetic body force.

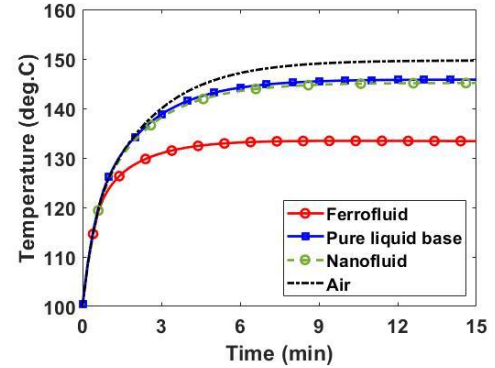


Fig. 15. Maximum coil temperatures vs time for different coolants at rated current density of 18.4 A/mm<sup>2</sup>.

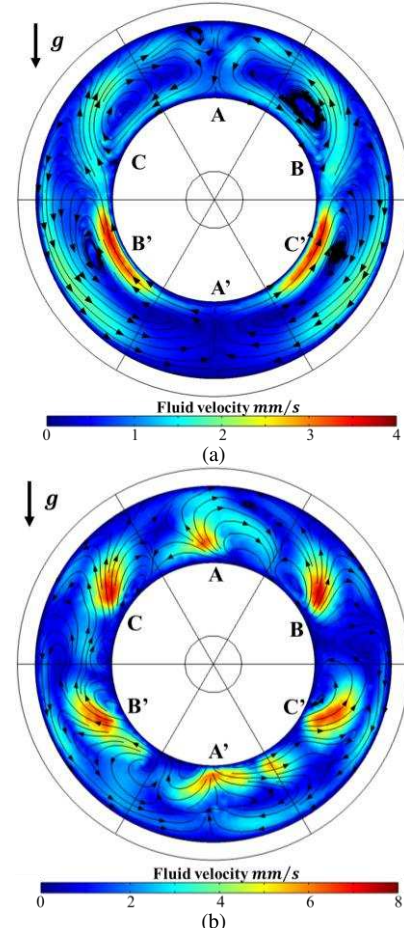


Fig. 16. Fluid flow velocity on plane 1 for (a) nanofluid and (b) ferrofluid at rated current density of 18.4 A/mm<sup>2</sup>.

The nanofluid with the same physical properties as those of the ferrofluid is affected by the same gravitational effect. Due to significant thermal expansion, the density of hotter fluid reduces and moves to the top sections (A, B and C) by buoyancy, whilst the cooler fluid moves towards the bottom sections (A', B' and C'), as shown in Fig. 16 (a). The fluid behavior is also reflected in the coolant temperature as shown in Fig. 17 (a). Compared to the natural air cooling, this heat exchange helps the nanofluid to reduce the machine temperature by 4.8 °C. In addition, buoyancy also causes a circumferential asymmetry within the fluid flow and therefore an asymmetry of the machine temperature distribution, as listed in Table VI. The hotter coolant is gathered in the top sections, leading to higher temperature in these sections. It is worth noting that, the temperature reductions by the nanofluid and the pure liquid base are almost the same, as listed in Table VI. This is mainly because although the additional nanoparticles improve the conduction coefficient and increase the fluid viscosity, the low concentration of nanoparticles (e.g., 5.4%) very much limits their impact on fluid physical properties.

In addition to the gravitational effect, the magnetic body force can further reduce machine temperature. Compared with the nanofluid cooling, the ferrofluid can reduce the peak coil temperature by another 11.4°C, as shown in Fig. 17. The reason is that, due to the existence of magnetic body force, the circulation of the ferrofluid is faster, leading to increased thermomagnetic convection. In addition, the ferromagnetic particles are attracted to the center of the coil in each section as shown in Fig. 16 (b), resulting in more uniform distribution of coolant velocity field, and hence more uniform end-winding temperature distribution.

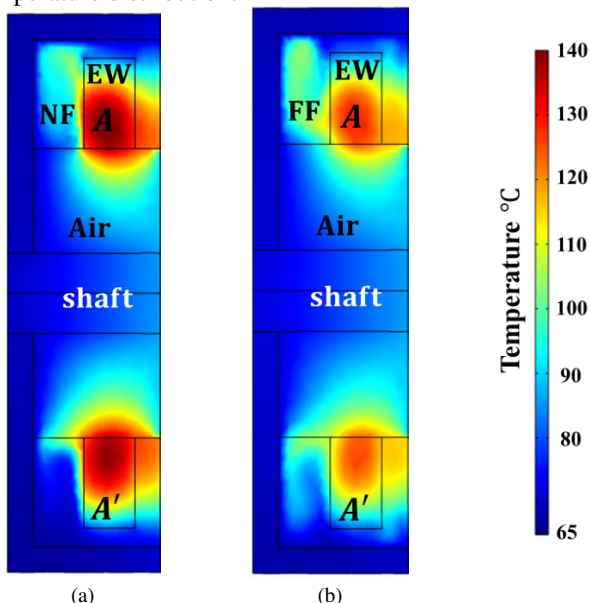


Fig. 17. Temperature distribution on plane 2 in the end-winding region for (a) nanofluid (NF) and (b) ferrofluid (FF) at rated current density of 18.4 A/mm<sup>2</sup>.

TABLE VI MAXIMUM COIL TEMPERATURES (IN °C) IN EACH SECTION

Coolant material	A	B	C'	A'
Ferrofluid	133.0	133.4	132.0	129.62
Nanofluid	144.8	144.8	143.5	142.5
Pure liquid base	145.7	145.6	144.5	143.5
Air	149.6	149.6	149.6	149.6

## B. Different Ferrofluid Material Properties

The section above confirms the ability of ferrofluid in improving the cooling performance of electrical machines. This improvement is due to the existence of the nano-sized ferromagnetic particles in the liquid base as (1) they improve the thermal conductivity; (2) they improve the gravitational effect due to higher thermal expansion; and (3) they can also lead to significant thermomagnetic convection due to magnetic body force. The improvement can be further enhanced by increasing the concentration of ferromagnetic particles or using materials with better temperature dependent magnetization properties, as will be investigated in following sections.

### a. Concentration

Increasing the concentration can improve the cooling efficiency for both the nanofluid and ferrofluid. However, the temperature reduction by the ferrofluid is more significant, as can be seen in Fig. 18. It is found that compared to a concentration of 0%, i.e., the pure liquid base, the coil temperatures are reduced by only 1.1% when the concentration of the nanofluid is increased to 10%. The marginal temperature reduction is due to slightly increased thermal conductivity and expansion coefficient and hence an enhanced gravitational effect. This is the same case for the ferrofluid. However, the thermomagnetic convection obtained by introducing the ferromagnetic particles can further reduce the machine temperature. The boosted magnetic body force due to a higher concentration as derived in (7) leads to a quicker coolant circulation and a larger thermomagnetic convection. As a result, the coil temperatures can be reduced by 11.7% when the concentration of the ferrofluid is 10%.

Although the thermomagnetic convection can be enhanced by increasing the concentration, the concentrations of the ferrofluid in literature are mostly around 5%. This is because higher concentration also increases the interaction between ferromagnetic particles. This could increase their agglomeration and make the fluid unstable. Therefore, ferrofluids with a concentration of up to 10% has been selected for the investigations in this paper.

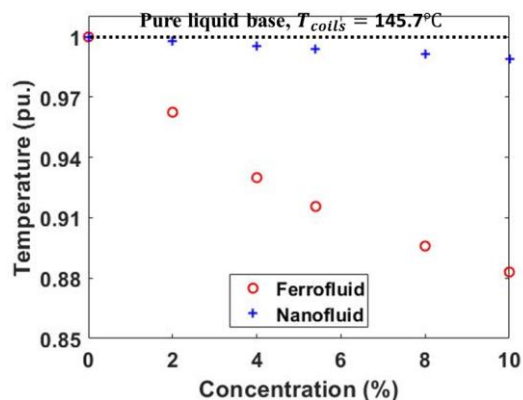


Fig. 18. Normalized maximum coil temperatures for different concentrations of ferrofluid at rated current density of 18.4 A/mm<sup>2</sup>.

### b. Saturation Magnetization and Curie Temperature

Previous results demonstrated the significant role of the thermomagnetic convection in improving machine thermal performance. It is also found that increasing the magnetic

body force is an efficient method to improve the thermomagnetic convection, and hence the cooling efficiency of the ferrofluid. The magnetic body force in (3) and (7) shows that it is affected by the temperature dependent magnetization curve. Since the magnetization curve is the intrinsic properties of materials, different ferromagnetic materials are chosen to investigate the influence of the magnetization curve. Their magnetic properties, i.e., saturation magnetization ( $M_0$ ) at 20°C and Curie Temperature ( $T_c$ ) are listed in Table VII. According to (3) and (4), higher  $M_0$  leads to higher magnetic susceptibility, while higher  $T_c$  also leads to higher susceptibility and lower reduction rate of susceptibility, as shown in Fig. 19. It is worth noting that the operating temperature of the ferrofluid in this study is within the range between 70°C and 110°C, as shown in the shaded region in Fig. 19.

The maximum coil temperatures for ferrofluid with different ferromagnetic particles are shown in Fig. 20. It is found that  $Fe_3O_4$  achieve lower temperatures due to their higher susceptibilities within the selected operating temperature range. However, the highest temperature is achieved by  $CdMn_2$  because its Curie temperature is far lower than the selected operating temperature range as listed in Table VII. This means that this kind of ferrofluid is fully demagnetized in the selected operating temperature range, and therefore cannot generate magnetic body force from the external magnetic field as described by (7). Regarding the cooling performances of  $GdCO_2$  and Ni, an interesting phenomenon has been observed.  $GdCO_2$  has similar susceptibility at 100°C as Ni, whilst its susceptibility reduces much faster when temperature increases. This means that, compared to Ni,  $GdCO_2$  may produce lower magnetic body force under the same magnetic field. However, the coil temperature cooled by ferrofluid using  $GdCO_2$  is much lower than that cooled by ferrofluid using Ni. This interesting phenomenon is because  $GdCO_2$  subjects to almost the same magnetic body force as Ni in the colder region, but lower magnetic body force in the hotter region. This larger magnetic body force gradient leads to faster coolant circulation, and hence lower machine temperature.

TABLE VII  $M_0$  AND  $T_c$  FOR DIFFERENT FERROMAGNETS [30]

	$Fe_3O_4$	Ni	$GdCO_2$	$CoFe_2O_4$	$CdMn_2$
$M_0$ (kA/m)	875	484	517	387	215
$T_c$ (°C)	500	358	180	520	30

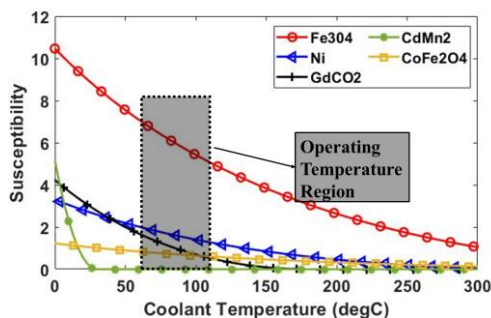


Fig. 19. Magnetic susceptibility curve of different ferromagnets.

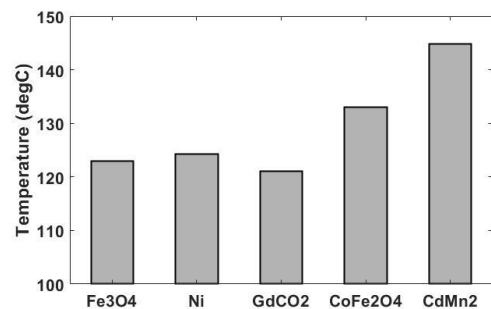


Fig. 20. Maximum coil temperatures with different ferrofluids at rated current density of 18.4 A/mm<sup>2</sup>.

### C. Different Electrical Loadings

Previous results demonstrated that the ferrofluid in end-winding region can improve the machine cooling performance. This means that, without exceeding the maximum allowable temperature of insulations, higher phase current (or electrical loading) may be injected to achieve higher machine power density. When the phase current increases, the copper loss will be increased accordingly, and the advantage of adopting ferrofluid cooling will be more pronounced, as can be seen from Fig. 21. This is mainly because the increased current density improves both the gravitational effect and the magnetic body force, and hence improves the thermomagnetic convection.

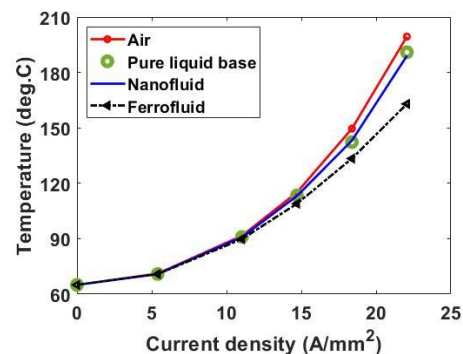


Fig. 21. Maximum coil temperatures at steady state vs current density for different coolants.

As mentioned in the section V. A, the gravitational effect can be investigated separately from the thermomagnetic convection by studying the results obtained using the nanofluid as coolant. It is found that when the current density is increased from 18.4 A/mm<sup>2</sup> to 22.1 A/mm<sup>2</sup>, the coolant flow velocity for the machine with nanofluid cooling increases from 3.66 mm/s [Fig. 16 (a)] to 4.93 mm/s [Fig. 22 (a)]. This is because a larger temperature gradient within the nanofluid is achieved for machines with increased current density (and increased copper loss). To be more specific, the temperature gradient is increased from 65.1 °C [Fig. 17 (a)] to 98.84 °C [Fig. 23 (a)] when current density is increased from 18.4 A/mm<sup>2</sup> to 22.1 A/mm<sup>2</sup>.

Regarding the magnetic body force attributing to the thermomagnetic convection, according to (7), it also increases at a higher current density due to higher magnetic field intensity in the end-winding region. Consequently, the coolant flow velocity increases, leading to increased thermomagnetic convection. When the current density rises from 18.4 A/mm<sup>2</sup> to 22.1 A/mm<sup>2</sup>, the maximum coolant velocity for the

machine with ferrofluid cooling is increased from 7.47 mm/s [Fig. 16 (b)] to 11.3 mm/s [Fig. 22 (b)]. As a result, a much more significant temperature reduction (by 36.4 °C compared with air cooling) can be achieved, as shown in Fig. 23 (b). This large temperature reduction is mainly attributed to much higher magnetic body force at high current density, which accounts for 26 °C. The remaining and relatively minor temperature reduction is attributed to the gravitational effect, which accounts for 10.4 °C.

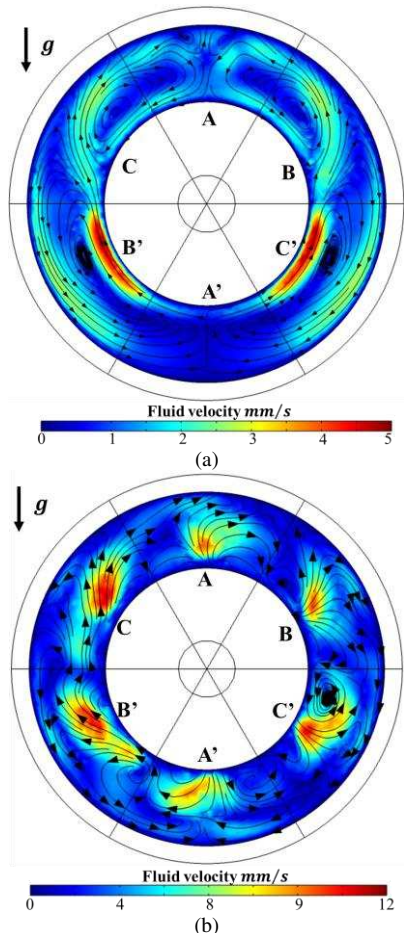


Fig. 22. Fluid flow velocity on plane 1 for (a) nanofluid and (b) ferrofluid when the current density is 22.1 A/mm<sup>2</sup>.

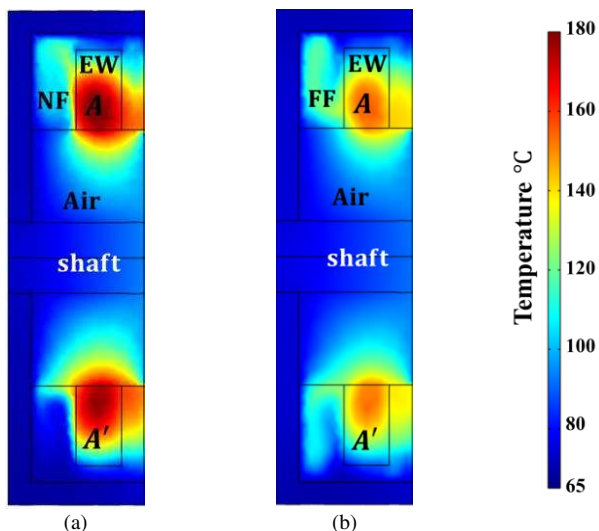


Fig. 23. Temperature distribution on plane 2 for (a) nanofluid (NF) and (b) ferrofluid (FF) when the current density is 22.1 A/mm<sup>2</sup>.

## VI. CONCLUSION

A hybrid cooling technology that combines ferrofluid (for end-windings cooling) and housing water jacket has been proposed and investigated in this paper. 3D multiphysics models using COMSOL have been developed for the simulations. The temperature and magnetic field dependent ferrofluid properties, e.g., magnetization, viscosity, density and thermal conductivity and capacity, have been considered in the 3D multiphysics models to predict the behavior of ferrofluid in the end-winding region. It is found that the ferrofluid under external magnetic field generated by the windings will mainly be driven by the magnetic body force. The circulation of the ferrofluid will lead to thermomagnetic convection, which enhances the heat transfer between the end-winding and the housing. The results obtained using the developed multiphysics model have shown that, together with the gravitational effect, the ferrofluid can reduce the maximum coil temperatures by 16.2 °C when the current density is 18.4 A/mm<sup>2</sup>. When the current density increases, the temperature reduction using ferrofluid cooling is more pronounced. For example, when the current density is 22.1 A/mm<sup>2</sup>, the peak temperature can be reduced by around 36.4 °C, in which 26 °C is attributed to the magnetic body force and 10.4 °C results from the gravitational effect.

The influence of ferrofluid properties on machine cooling performance has also been investigated. It is found that increasing the concentration of ferrofluid can significantly reduce the peak temperature. This improved cooling performance is mainly attributed to the increase in magnetic body force, which leads to improved thermomagnetic convection. In addition, increasing concentration slightly increases the thermal conductivity and the gravitational effect, which also helps improve machine cooling performance. Similarly, the magnetization of ferrofluid also affects the cooling performance. It is found that the ferrofluid with higher magnetization within the selected machine operating temperature range has better cooling performance due to its higher magnetic body force, and hence more significant thermomagnetic convection. In addition, a faster reduction rate of magnetization when temperature rises will provide a larger gradient of magnetic body force within the ferrofluid, leading to a faster coolant circulation and hence a better machine cooling performance. A motorette has been built and the multiphysics models have been validated by a series of experiments.

## VII. REFERENCE

- [1] S. Grubic, J. M. Aller, B. Lu, and T. G. Habetler, "A survey on testing and monitoring methods for stator insulation systems of low-voltage induction machines focusing on turn insulation problems," *IEEE Trans. Ind. Electron.*, vol. 55, no. 12, pp. 4127-4136, 2008.
- [2] M. Popescu, D. Staton, D. Dorrell, F. Marignetti, and D. Hawkins, "Study of the thermal aspects in brushless permanent magnet machines performance," in *2013 IEEE WEMDCD*, Mar. 2013: IEEE, pp. 60-69.
- [3] M. Popescu, D. Staton, A. Boglietti, A. Cavagnino, D. Hawkins, and J. Goss, "Modern heat extraction systems for electrical machines-A review," in *2015 IEEE WEMDCD*, 2015: IEEE, pp. 289-296.
- [4] A. Boglietti, A. Cavagnino, D. Staton, M. Shanel, M. Mueller, and C. Mejuto, "Evolution and modern approaches for thermal analysis of electrical machines," *IEEE Trans. Ind. Electron.*, vol. 56, no. 3, pp. 871-882, 2009.

- [5] D. A. Staton and A. Cavagnino, "Convection heat transfer and flow calculations suitable for electric machines thermal models," *IEEE Trans. Ind. Electron.*, vol. 55, no. 10, pp. 3509-3516, 2008.
- [6] X. Fan, D. Li, R. Qu, C. Wang, and H. Fang, "Water cold plates for efficient cooling: Verified on a permanent-magnet machine with concentrated winding," *IEEE Trans. Ind. Electron.*, vol. 67, no. 7, pp. 5325-5336, 2019.
- [7] Y. Gai, M. Kimiabeigi, Y.C. Chong, J.D. Widmer, J. Goss, U. SanAndres, A. Steven, D.A. Staton, "On the measurement and modeling of the heat transfer coefficient of a hollow-shaft rotary cooling system for a traction motor," *IEEE Trans. Ind. Appl.*, vol. 54, no. 6, pp. 5978-5987, 2018.
- [8] Y. C. Chong, E. J. E. Subiabre, M. A. Mueller, J. Chick, D. A. Staton, and A. S. McDonald, "The ventilation effect on stator convective heat transfer of an axial-flux permanent-magnet machine," *IEEE Trans. Ind. Electron.*, vol. 61, no. 8, pp. 4392-4403, Aug. 2013.
- [9] R. Zhou, G. Li, Z. Zhu, M. Foster, and D. Stone, "Improved cooling in modular consequent pole PM machine utilizing flux gaps," in *2020 IEEE ECCE*, 2020: IEEE, pp. 4253-4260.
- [10] R. Zhou, G.J. Li, Z.Q. Zhu, M.P. Foster, D.A. Stone, C.J. Jia and P. McKeever, "Novel Liquid Cooling Technology for Modular Consequent-Pole PM Machines," in *2021 IEEE IEMDC*, 2021: IEEE, pp. 1-7.
- [11] Z. Xu, A. La Rocca, P. Arumugam, S.J. Pickering, C. Gerada, S. Bozhko, D. Gerada and H. Zhang, "A semi-flooded cooling for a high speed machine: Concept, design and practice of an oil sleeve," in *IECON 2017-43rd Annual Conf. IEEE Ind. Electron. Soc.*, 2017: IEEE, pp. 8557-8562.
- [12] G. Liang and I. Mudawar, "Review of spray cooling—Part 1: Single-phase and nucleate boiling regimes, and critical heat flux," *Int. J. Heat Mass Trans.*, vol. 115, pp. 1174-1205, 2017.
- [13] C. Liu, Y. C. Chong, M. Michon, J. Goss, D. Gerada, Z. Y. Xu, C. Gerada, H. Zhang., "Model calibration of oil jet and oil spray cooling in electrical machines with hairpin windings," in *2021 IEEE ECCE*, 2021: IEEE, pp. 3813-3820
- [14] M. Taniguchi *et al.*, "Development of new hybrid transaxle for compact-class vehicles," SAE Technical Paper, 0148-7191, 2016 2016.
- [15] M. Popescu, J. Goss, D. A. Staton, D. Hawkins, Y. C. Chong, and A. Boglietti, "Electrical vehicles—Practical solutions for power traction motor systems," *IEEE Trans. Ind. Appl.*, vol. 54, no. 3, pp. 2751-2762, 2018.
- [16] C. Liu, Z. Y. Xu, D. Gerada, J. Li, C. gerada, Y. C. Chong, M. Popescu, J. Goss, D. Staton, H. Zhang, "Experimental investigation on oil spray cooling with hairpin windings," *IEEE Trans. Ind. Electron.*, vol. 67, no. 9, pp. 7343-7353, 2019.
- [17] V. Madonna, A. Walker, P. Giangrande, G. Serra, C. Gerada, and M. Galea, "Improved thermal management and analysis for stator end-windings of electrical machines," *IEEE Trans. Ind. Electron.*, vol. 66, no. 7, pp. 5057-5069, 2018.
- [18] C. Micallef, S. Pickering, K. Simmons, and K. Bradley, "An alternative cooling arrangement for the end region of a totally enclosed fan cooled (TEFC) induction motor," 2008, 2008.
- [19] M. Kang, H. Wang, L. Guo, T. Shi, and C. Xia, "Self-circulation cooling structure design of permanent magnet machines for electric vehicle," *Appl. Therm. Engin.*, vol. 165, p. 114593, 2020.
- [20] M. Polikarpova, P. Ponomarev, P. Lindh, I. Petrov, W. Jara, V. Naumanen, J. A. Tapia, J. Pyrhonen, "Hybrid cooling method of axial-flux permanent-magnet machines for vehicle applications," *IEEE Trans. Ind. Electron.*, vol. 62, no. 12, pp. 7382-7390, 2015.
- [21] W. Lian, Y. Xuan, and Q. Li, "Characterization of miniature automatic energy transport devices based on the thermomagnetic effect," *Energy Conversion and Management*, vol. 50, no. 1, pp. 35-42, 2009.
- [22] M. Petit, Y. Avenas, A. Kedous-Lebouc, W. Cherief, and E. Rullière, "Experimental study of a static system based on a magneto-thermal coupling in ferrofluids," *Int. J. refrigeration*, vol. 37, pp. 201-208, 2014.
- [23] S. N. El Dine, X. Mininger, C. Nore, R. Zanella, F. Bouillault, and J.-L. Guermont, "Impact of Magnets on Ferrofluid Cooling Process: Experimental and Numerical Approaches," *IEEE Trans. Magn.*, vol. 56, no. 1, pp. 1-4, Dec. 2019.
- [24] R. Zanella, C. Nore, X. Mininger, F. Bouillault, and J.-L. Guermont, "Numerical Study of Cooling by Ferrofluids in an Electrical Transformer using an Axisymmetric Model," *IEEE Trans. Magn.*, 2021.
- [25] L. Pislaru-Danescu, A. M. morega, M. Morega, V. Stoica, O. M. Marinica, F. Nouras, N. Paduraru, I. Borbath, T. Borbath, "Prototyping a ferrofluid-cooled transformer," *IEEE Trans. Ind. Appl.*, vol. 49, no. 3, pp. 1289-1298, 2013
- [26] J. Patel, K. Parekh, and R. Upadhyay, "Prevention of hot spot temperature in a distribution transformer using magnetic fluid as a coolant," *Int. J. Therm. Sci.*, vol. 103, pp. 35-40, May 2016.
- [27] G. Karimi-Moghaddam, R. D. Gould, S. Bhattacharya, and D. D. Tremelling, "Thermomagnetic liquid cooling: A novel electric machine thermal management solution," in *2014 IEEE ECCE*, Sep. 2014: IEEE, pp. 1482-1489.
- [28] R. E. Rosensweig, "Magnetic fluids," *Ann. Rev. Fluid Mech.*, vol. 19, no. 1, pp. 437-461, 1987.
- [29] S. W. Charles, "The preparation of magnetic fluids," in *Ferrofluids*: Springer, 2002, pp. 3-18.
- [30] B. Berkovsky, V. F. Medvedev, and M. S. Krakov, *Magnetic fluids: engineering applications*. New York, USA: Oxford Univ, 1993.
- [31] S. Chikazumi and C. D. Graham, *Physics of Ferromagnetism* (no. 94). London, UK: Oxford Univ. Press, 2009.
- [32] M. Kaviany, *Essentials of heat transfer: principles, materials, and applications*. New York, USA: Cambridge Univ. Press, 2011.